BRACELET BUS-NA 98 BZ 11 - BRONZE - IRON AGE - SWITZERLAND

Artefact name Bracelet bus-na 98 BZ 11

Authors Christian. Degrigny (HE-Arc CR, Neuchâtel, Neuchâtel, Switzerland) & Naima. Gutknecht (HE-Arc CR, Neuchâtel, Neuchâtel, Switzerland) & Valentina. Valbi (Laboratoire Métallurgie et Culture LMC-IRAMAT-CNRS-UTBM, Belfort, Franche-Comté, France)

Url /artefacts/1000/

The object

Credit Service archéologique de l'Etat de Fribourg, M-J.Scholl.

Fig. 1: Bracelet bus-na 98 BZ 11 side A from Bussy/Pré de Fond (Switzerland),

Description and visual observation

Description of the artefact Fragment of a deburred bracelet with irregular curvature and triangular section, surface of side A with a central rib and hammer marks and surface of side B flat.

Type of artefact Jewellery

Origin Bussy/Pré de Fond, Fribourg, Fribourg, Switzerland

Recovering date 1998

Chronology category Iron Age

chronology tpq 550 B.C.

chronology taq 450 B.C.

Chronology comment	First Iron Age - Hallstatt Culture (Ha D2-3)
Burial conditions / environment	Soil
Artefact location	Archaeological Service of the Fribourg Canton, Fribourg
Owner	Archaeological Service of the Fribourg Canton, Fribourg
Inv. number	bus-na 98 BZ 11
Recorded conservation data	Mechanical cleaning of the external corrosion products and soils

Complementary information

This bracelet is part of a corpus of four bracelets (***bracelets bus-na 98 BZ 11 / bus-na 98 BZ 23 / bus-na 98 BZ 38 / bus-na 98 BZ 67***) found on the same site.

Study area(s)

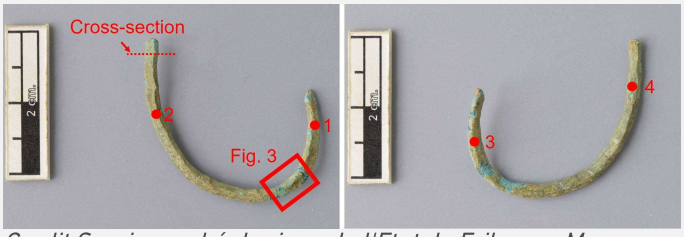

Credit Service archéologique de l'Etat de Fribourg, M-J.Scholl/HE-Arc CR, N.Gutknecht.

Fig. 2: Side B (left) and side A (right) of bracelet with location of the detail of Fig. 3 and showing the sampling area and the XRF analysis areas (red dots),

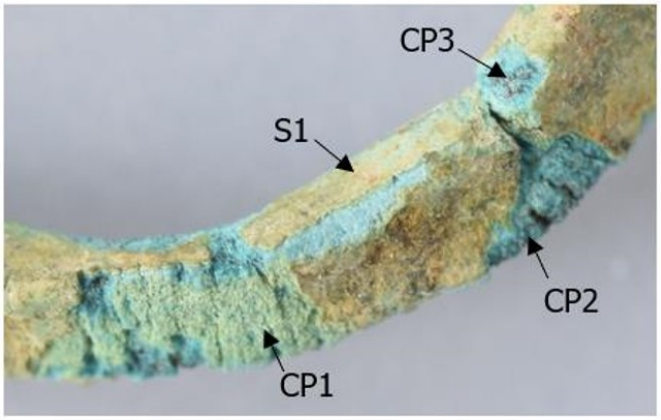

Credit HE-Arc CR, N.Gutknecht.

Fig. 3: Detail of the corrosion structure from Fig. 2 showing the documented strata,

Binocular observation and representation of the corrosion structure

The schematic representation below gives an overview of the corrosion structure encountered on the bracelet from a first visual macroscopic observation.

Strata	Type of stratum	Principal characteristics
S1	Soil	light brown, thin, non-compact, powdery
CP1	Corroded product	green, thin, discontinuous, compact, soft

CP2	Corroded product	blue, thick, discontinuous, non-compact, very soft
CP3	Corroded product	red, thin, continuous, compact, very soft
M1	Metal	orange, metallic, soft

Table 1: Description of the principal characteristics of the strata as observed under binocular and described according to Bertholon's method.

The transition between CP3 and the metal M1 is irregular and rough. There are cracks through S1, CP1 and CP2 that generate the flaking of CP1 and CP2.

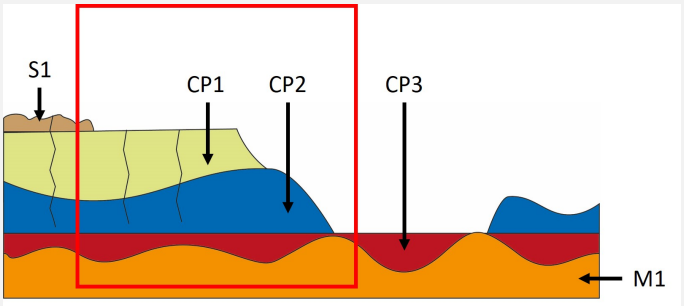

Credit HE-Arc CR, N.Gutknecht.

Fig. 4: Stratigraphic representation of the corrosion structure of the bracelet by macroscopic and binocular observation with indication of the corrosion structure used to build the MiCorr stratigraphy of Fig. 5 (red square),

MiCorr stratigraphy(ies) – Bi

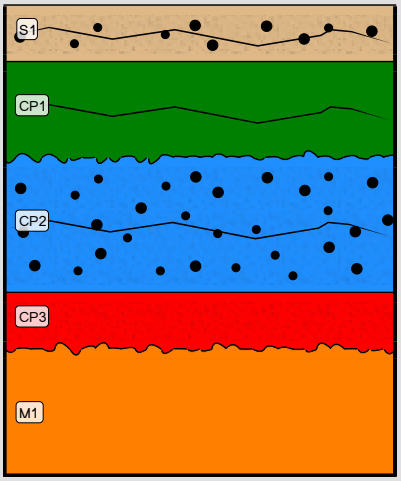

Fig. 5: Stratigraphic representation of the corrosion structure of the bracelet observed macroscopically under binocular microscope using the MiCorr application with reference to Fig. 4. The characteristics of the strata are only accessible by clicking on the drawing that redirects you to the search tool by stratigraphy representation, Credit HE-Arc CR, N.Gutknecht.

Sample(s)

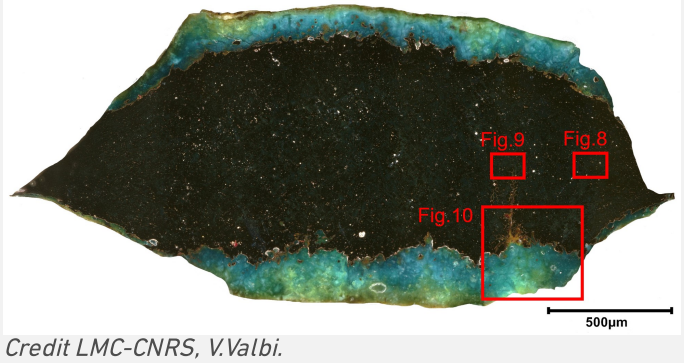

Credit LMC-CNRS, V.Valbi.

Fig. 6: Micrograph of the cross-section of the sample in dark field taken from the bracelet (Fig. 2) in dark field showing the location of Figs. 8 to 10,

Description of sample	The cross-section corresponds to a lateral cut (Fig. 2) and is representative of the entire thickness of the bracelet's body. A metallic core is present below the corrosion layers (Fig. 6).
Alloy	Bronze
Technology	Cold worked with repeated annealing and final cold working
Lab number of sample	ébauche 11
Sample location	Archaeological Service of the Fribourg Canton, Fribourg
Responsible institution	Archaeological Service of the Fribourg Canton, Fribourg
Date and aim of sampling	February 2020. Metallographic study.

Complementary information

None.

Analyses and results

Analyses performed:

Non-invasive approach

- XRF with handheld portable X-ray fluorescence spectrometer (NITON XL3t 950 Air GOLDD+, Thermo Fischer®). General Metal mode, acquisition time 60s (filters: Li20/Lo20/M20).

Invasive approach (on the sample)

- Optical microscopy: the sample is polished, then it is observed on a numerical microscope KEYENCE VHX-7000 in bright and dark field.
- Metallography: the polished sample is etched with alcoholic ferric chloride and observed by optical microscopy in bright field.
- SEM-EDS: the sample is coated with a carbon layer and analyses are performed on a SEM-FEG JEOL 7001-F equipped with a silicon-drift EDS Oxford detector (Aztec analysis software) with an accelerating voltage of 20 kV and probe current at about 9 nA. The relative error is considered of about 10% for content range <1mass%, and of 2% for content range of >1mass%.
- µ-Raman spectroscopy: it is performed on a HORIBA Labram Xplora spectrometer equipped with a 532 nm laser with 1800 grating, the laser power employed is between 0.04 and 0.55 mW with acquisition time varying between 1 and 5 minutes.

Non invasive analysis

The XRF analysis of the bracelet was carried out before sampling on four areas (Fig. 2). All strata (soil, corrosion products, and metal) are analyzed at the same time. The metal is presumably a copper-tin alloy with some lead (and perhaps Bi), while the other elements detected (Fe, Si, P, Al) are from the burial environment.

Elements (mass %)	1	2	3	4
Cu	40	28	33	27
Sn	39	44	39	43
Pb	2	2	2	3
Bi	1	1	1	1
Fe	6	13	8	14
Si	6	5	9	5
P	3	5	2	5

Al	2	>2	3	2

Table 2: Chemical composition of the surface of the bracelet at four representative points shown in Fig.2. Method of analysis: XRF. The results are rounded up to the nearest whole number.

Metal

EDX analysis (Table 3) of the residual metal on cross-section indicates that it is a low tin bronze (7-8 mass% Sn) with a low percentage of Pb (0.5 mass%).

The metal etched with alcoholic ferric chloride reveals a main equiaxe grain structure (Fig. 7) with several twinned grains (Figs. 8 and 9), indicating that the object underwent an annealing procedure. It is possible to observe on the thinner extremities of the sample the deformation of the grains (shown for the right extremity on Fig. 8) and the presence of slip lines (Fig. 8) caused by cold mechanical working of the metal after annealing.

Small Pb inclusions (2-3 µm, Figs. 8-9) are homogeneously distributed on the whole surface of the sample.

Intergranular corrosion is observed (Fig. 9), as well as a thick transgranular fracture.

Elements	mass %
Cu	91
Sn	7.8
Pb	0.5
As	<0.5
Ni	<0.5
Al	<0.5
Si	<0.5

Table 3: Chemical composition (mass %) of the alloy over a general area of analysis obtained by SEM-EDX.

Credit LMC-CNRS, V.Valbi.

Fig. 7: Micrograph of the etched cross-section of the sample taken from the bracelet (Fig. 2) in bright field,

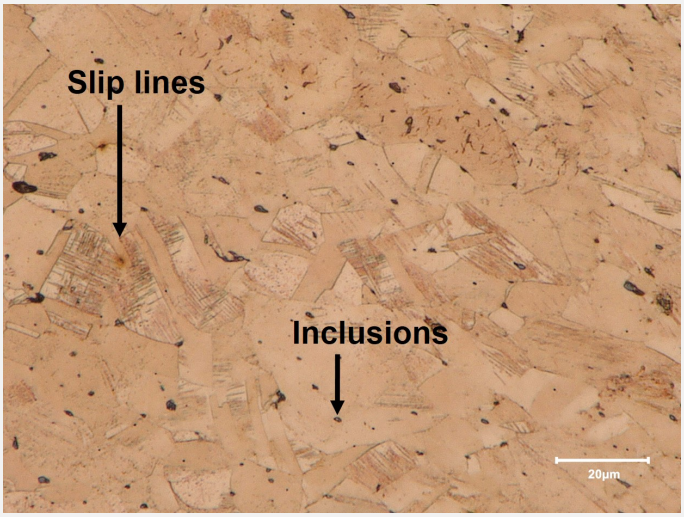

Fig. 8: Micrograph of the metal sample from Fig. 6 (detail), etched, bright field. Elongated grains with slip lines are observed, as well as grey lead inclusions,

Credit LMC-CNRS, V.Valbi.

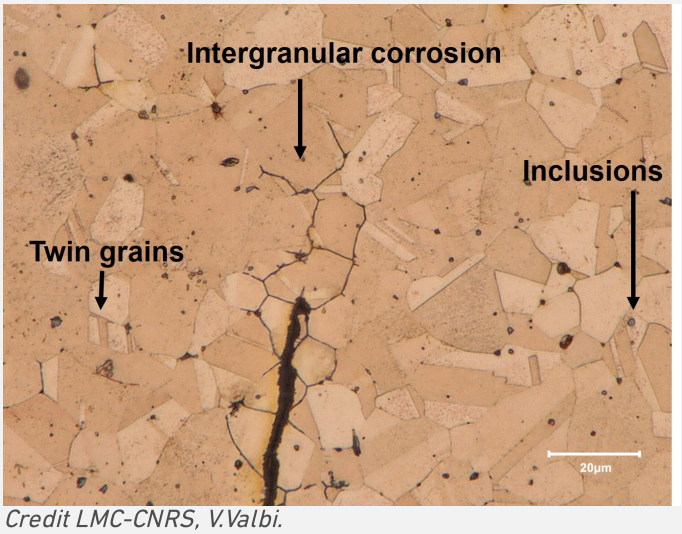

Credit LMC-CNRS, V.Valbi.

Fig. 9: Micrograph of the metal sample from Fig. 6 (detail), etched, bright field. Twin grains and Pb inclusions are observed as well as intergranular corrosion,

Microstructure	Polygonal grains with twinned and strain lines
First metal element	Cu
Other metal elements	Sn, Pb

Complementary information

The interface roughness between the metal and the CPs, corresponding to the stratum identified as corroded metal (CM1) was measured through optical microscopy observation and the following parameters were determined (in µm): Rp=56, Rv = 68, Rt = 124, Ra = 41.

Corrosion layers

The observation of the sample in cross-section in dark field allowed identification of an external discontinuous greenish/yellowish stratum (CP1), a blue stratum (CP2), a red discontinuous thin stratum (CP3) at the interface with the metal, and a corroded metal area (CM1)(Fig.2). This is confirmed in Fig. 10.

The EDX elemental analysis (Table 4) and mapping (Fig. 11) of the visually identified CPs by binocular and cross-sectional observations show that CP1 is Cu depleted, O, Sn and Pb enriched and polluted with Ca, Fe and P, while CP2 is also Cu depleted and O and Sn-rich but with fewer external polluting elements and CP3 is Cu rich. The results are in agreement with those of the preliminary XRF analysis (table 2), with the exception of aluminum and bismuth which are apparently contained only in S1. Indeed, the XRF analysis indicates tin and Pb enrichments on the four areas investigated of the metal surface.

	CP1	CP2	CP3
Cu	16.2	28.4	57.6
Sn	33.6	34.7	18.2
O	32.4	30.2	18.1
Pb	1.3	0.8	0.7
Si	1.6	1.9	0.9
P	5.0	2.4	1.8
Fe	6.5	< 0.5	< 0.5
Ca	2.8	0.9	< 0.5
Cl	< 0.5	< 0.5	0.8

Table 4: Chemical composition (mass%) of the corrosion layers over a general area of analysis in cross-section obtained by SEM-EDX.

Analyses with µ-Raman were performed on the three identified strata (Fig. 11). The R01 (Fig. 12) point of analysis was performed on the red CP3 layer and the obtained spectrum presented the typical main peaks (145, 218, 632 cm^{-1}) of the Raman RUFF reference spectrum of cuprite Cu_2O (Lafuente et al. 2015). The R02 point of analysis was performed on the blue layer and the spectrum obtained has a broad peak at 560 cm^{-1} that can be attributed to nanocrystals of cassiterite Sn_2O thanks to comparison with the work of Ospitali et al. 2012. The R03 analysis point performed on the green/yellow external phase was too disturbed by fluorescence signal and an identification of the phase was impossible. The blue color of CP2 is probably caused by residual Cu ions, while the greenish/yellowish color of CP1 is given by the presence of Fe ions.

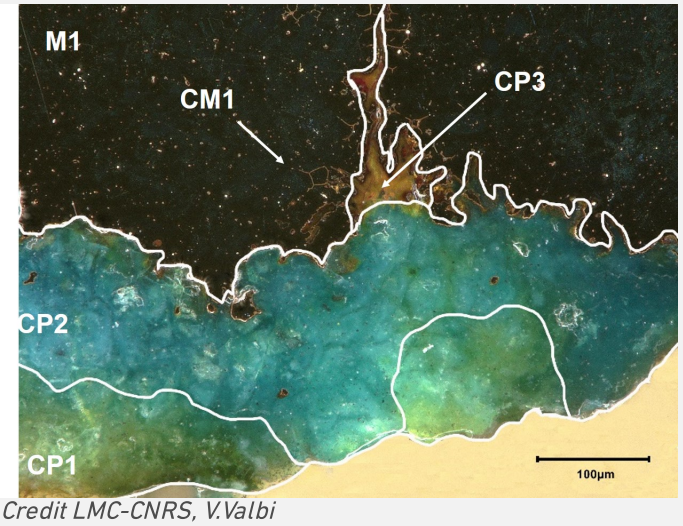

Credit LMC-CNRS, V.Valbi

Fig. 10 : Micrograph of the corrosion structure from Fig. 6 (detail) with the subdivision of the different strata, unetched, dark field,

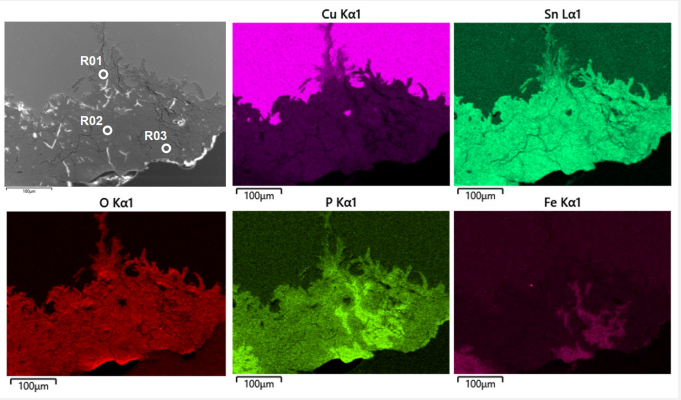

Credit LMC-CNRS, V.Valbi.

Fig. 11: SEM image, BSE-mode, and elemental chemical distribution of Fig.10. The selected points for Raman analysis shown in Fig. 12 are indicated,

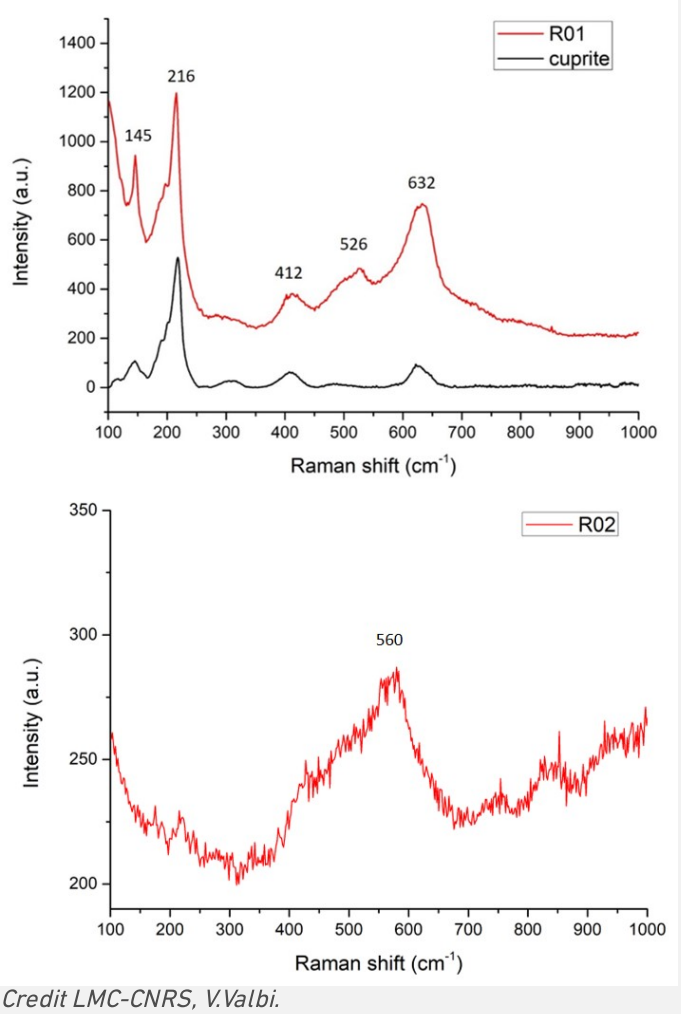

Fig. 12: Raman spectra of points R01 (together with the RRUFF reference RRUFFID=R140763 for cuprite) and R02 showed in Fig. 11,

Credit LMC-CNRS, V.Valbi.

Corrosion form	Uniform - intergranular
Corrosion type	Type I (Robbiola)

Complementary information

None.

MiCorr stratigraphy(ies) – CS

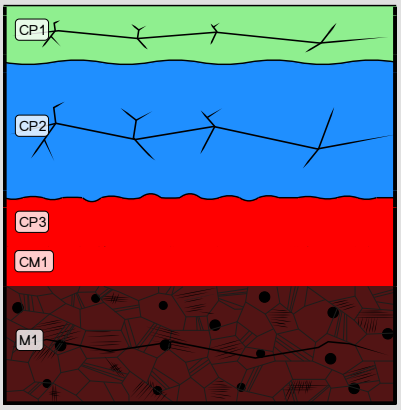

Fig. 13: Stratigraphic representation of the sample of bracelet observed in cross-section under dark field using the MiCorr application. The characteristics of the strata are only accessible by clicking on the drawing that redirects you to the search tool by stratigraphy representation. This representation was build according to Fig. 10, Credit LMC-CNRS, V.Valbi.

Synthesis of the binocular / cross-section examination of the corrosion structure

Three CPs were identified with both binocular and cross-sectional observations, but some differences between the two methods of observation should be noted. The outer sediment layer (S1), easily identified under binocular, was barely visible as a thin dark yellow layer in the cross-section and could have been interpreted as part of CP1 if observed only under cross-section.

On the contrary, the presence of a CM1 stratum was only revealed through cross-section observation. Moreover, information obtained under binocular examination such as brightness, compactness, cohesion, and adherence are not accessible during cross-sectional observation. Conversely, the physico-chemical characteristics obtained by cross-section examination are not easily accessible during the binocular examination. The differences observed underline the necessity and complementarity of these two approaches.

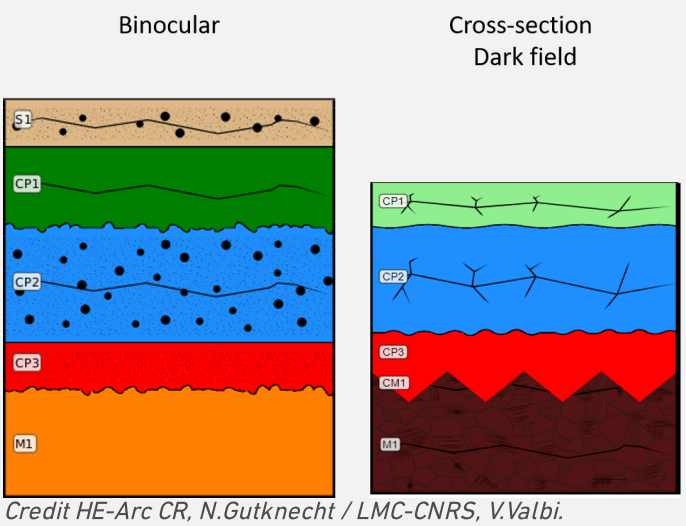

Credit HE-Arc CR, N.Gutknecht / LMC-CNRS, V.Valbi.

Fig. 14: Stratigraphic representation side by side of binocular view and cross-section (dark field),

Conclusion

The bracelet is a tin bronze with Pb inclusions. The metallographic observation revealed that the metal was annealed with final cold-working.

The characterization of the corrosion products showed a typical corrosion structure for an archeological bronze. The object presents the phenomenon of decuprification with Sn enrichment. This is a common phenomenon observed on bronze archaeological objects buried in moderately aggressive natural conditions (such as oxygenated sandy soils) and accompanied by the formation of cuprite at the interface with the metal. Cuprite is the first compound often to be formed during the corrosion of bronzes (Robbiola et al. 1998, Scott 2006). The local enrichment in Fe and P in the CP1 was also previously observed on archaeological objects (Robbiola et al. 1998, Papadopoulou et al. 2016) and can be attributed to the diffusion of these elements from the burial soil.

The limit of the original surface according to Bertholon's method is probably located on the upper interface between S1 and CP1. CP1 presents hammering traces which are typical markers of the original surface. This surface is partially lost due to the flaking of the layers CP1 and CP2. The conservation of the original surface allows to identify the corrosion form as a Type I according to Robbiola et al. 1998 classification.

This bracelet is part of a corpus of four bracelets (***bracelets bus-na 98 BZ 11 / bus-na 98 BZ 23 / bus-na 98 BZ 38 / bus-na 98 BZ 67***) found on the same site. These artefacts are all drafts of bracelets but correspond to different stages of advancement: two bracelets are "as cast" and present no further working (***bracelet bus-na 98 BZ 23*** and ***bus-na 98 BZ 38***) while two bracelets present signs of annealing and cold-working (***bracelet bus-na 98 BZ 11*** and ***bus-na 98 BZ 67***).

References

References on object and sample

1. MiCorr_Bracelet bus-na 98 BZ 23
2. MiCorr_Bracelet bus-na 98 BZ 38
3. MiCorr_Bracelet bus-na 98 BZ 67

References on analytical methods and interpretation

4. Lafuente, B., Downs, R. T., Yang, H., Stone, N. (2015) The power of databases: the RRUFF project. In: Highlights in Mineralogical Crystallography, T. Armbruster and R. M. Danisi, eds. Berlin, Germany, W. De Gruyter, 1-30.
5. Ospitali, F., Chiavari, C., Martini, C., Bernardi, E., Passarini, F., Robbiola, L. (2012) The characterization of Sn-based corrosion products in ancient bronzes: a Raman approach. Journal of Raman Spectrpscopy, 43 (11), 1596-1603.
6. Papadopoulou, O., Vassiliou, P., Grassini, S., Angelini, E. and Gouda, V. (2016) Soil-induced corrosion of ancient Roman brass – A case study. Materials and Corrosion, 67, No. 2.
7. Scott, D. (2006) Metallography and microstructure of ancient and historic metals. J Paul Getty Museum Publications.
8. Robbiola L., Blengino M., Fiaud C., (1998) Morphology and mechanisms of formation of natural patinas on archaeological Cu–Sn alloys.